Int. J. Electrochem. Sci., 10 **(2015)** 6030 - 6043

International Journal of
ELECTROCHEMICAL
SCIENCE
www.electrochemsci.org

Short Communication

Effect of Thermal and Chemical Treatment on Electrodeposited CdTe Thin Films for Solar Cell Applications

Marwa Fathy[1,*], *Shaimaa Elyamny*[1], *Siham Mahmoud*[2] *and Abd El-Hady B. Kashyout*[1]

[1]Electronic Materials Research Department, Advanced Technology and New Materials Research Institute, City of Scientific Research and Technological Applications (SRTA-City), New Borg El-Arab City, P.O. Box 21934, Alexandria, Egypt.
[2]Electronic Microscope and Thin films Department, Physics Division, National Research Center, 12311 Dokki, Giza, Egypt.
[*]E-mail: mfathy@mucat.sci.eg; mrwfathy@gmail.com

Received: 2 April 2015 / *Accepted:* 19 May 2015 / *Published:* 24 June 2015

Electrodeposition of nanocrystalline CdTe thin films from an acidic sulfate aqueous electrolyte was performed using different potential values to study the effect of the electrodeposition potential and thermal and chemical treatments on the structure, morphology and optical properties of the resulting films. Electrodeposition at -0.62 V(SCE) followed by heat and $CdCl_2$ treatment was used to produce CdTe films that showed a highly crystalline cubic structure, did not exhibit any free Te, had defined grains and free cracks and were nearly stoichiometric with a band gap of 1.44 eV. The properties of CdTe films were studied using X-ray diffraction (XRD), Raman spectroscopy, scanning electron microscopy (SEM), energy dispersive X-ray, and UV-Vis spectroscopy. The J –V characteristic curve of the CdTe/CdS solar cell was investigated under illumination intensity of 100 mW/cm^2. V_{oc} of 0.73 V, J_{sc} of 20 mA/cm^2, FF of 50%, and η of 9% were measured for the solar cell based on CdTe film that was electrodeposited at -0.62 V(SCE) and then treated by heat and $CdCl_2$.

Keywords: Nanocrystalline CdTe; electrodeposition; $CdCl_2$ and heat treatment, CdTe/CdS solar cell.

1. INTRODUCTION

Cadmium telluride (CdTe) has shown great promise for efficient, low-cost photovoltaic (PV) solar cells [1]. CdTe thin film solar cells have shown stable long-term performance and high efficiency [2]. CdTe has good properties as the absorber layer for the low cost photovoltaic cell [3] and has a direct band gap (1.44 eV) that is near the optimum for photovoltaic solar energy conversion [4]. The optical absorption coefficient of CdTe thin films is greater than 1 $\times 10^5$ cm^{-1}, sufficiently high to

achieve a nearly full absorption of light for thicknesses below 800 nm [5-6]. CdTe has been prepared using different techniques such as electrodeposition [7–8], closed-space sublimation (CSS) [9], spray pyrolysis [10], screen printing [11], atomic layer epitaxy [12] and radio-frequency (RF) sputtering [13].

Electrodeposition of CdTe has become a promising method for producing efficient thin film solar cells. The optimization of CdTe thin film and CdTe/CdS interface properties with post-deposition treatments is believed to play an important role in solar cell operation [14]. The $CdCl_2$ activation heat treatment is a critical processing step in the fabrication of high-efficiency CdTe-based solar cells. Due to the $CdCl_2$ activation heat treatment, CdTe films partially melt, re-grow and interface, the chlorine diffuses from the surface to the interior of the CdTe thin film and defects begin to be reduced [15-17]. The $K_2Cr_2O_7$:H_2SO_4 etching process leads to the removal of the oxide layer on the surface of CdTe [1].

In this paper, the structure, morphology, chemical composition and optical properties of CdTe thin films electrodeposited at different potential values on CdS/ITO/glass substrates before and after heat and $CdCl_2$ treatment were studied by X-ray diffraction (XRD), Raman spectroscopy, scanning electron microscopy (SEM), energy dispersive X-ray analysis (EDX) and UV-Vis spectrophotometer. Additionally, the J-V characteristics under illumination were measured to determine the solar cell characteristics and junction quality (J_{sc}, V_{oc}, and η).

2. EXPERIMENTAL WORK

2.1. Methodology

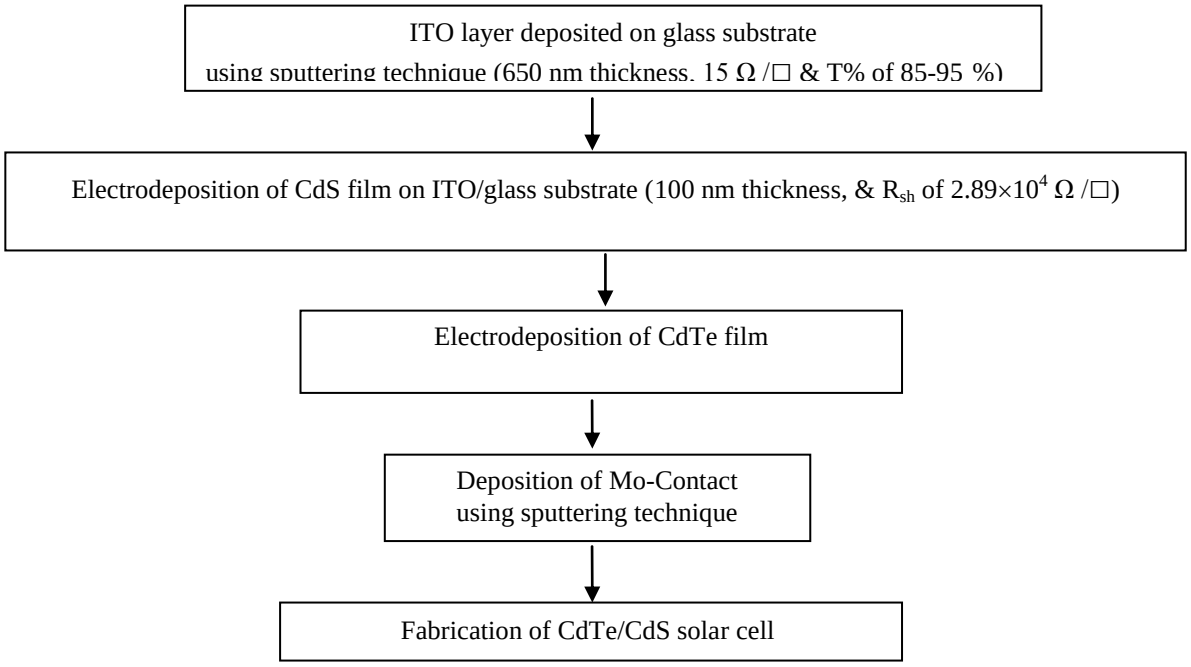

Figure 1. Flow chart of the experimental work.

The chart presented in Figure 1 explains the experimental procedure used in this work. Soda-lime glass substrates coated with 650 nm Indium-Tin Oxide (ITO) layer deposited by sputtering technique were used [18]. The substrates had a high transparency and a sheet resistance of approximately 15 Ω /□. Acetone, methanol and distilled water were used as cleaning solutions in an ultrasonic bath, and the samples were then dried under a stream of nitrogen. ITO glass substrates were immersed for 30 sec in 0.1 M HCl etching solution in order to remove impurities and increase the surface roughness and finally were washed in de-ionized water. CdS films were electrodeposited by the galvanostatic method, as reported in [19].

As-deposited CdS films were treated with $CdCl_2$:CH_3OH (0.5% of $CdCl_2$ by weight) solution. CdS films were dried, heat treated at 400˚C in air for 15 min, rinsed with distilled water and dried with nitrogen gas.

2.1.1. Electrodeposition of CdTe thin films

The CdTe thin films were electrodeposited by potentiostatic method from an aqueous solution of 1.5 M of $CdSO_4.(8/3)H_2O$ (Sigma Chemicals 99.97%) and 1 mM TeO_2 (Aldrich Chemicals 99.995%) [8]. The pH was adjusted to 1.6 by adding H_2SO_4. The bath temperature was kept constant at 80 ˚C and the stirring rate was approximately 300 rpm. A three-electrode cell was connected to a Wenking Potentio-Galvano-Scan (PGS 95). The reference electrode was a saturated calomel electrode (SCE), the working electrode was the CdS/ITO glass substrate and the counter electrode was a platinum sheet (2x2 cm^2). The deposition bath temperature was 80 °C, and a deposition time of 2 hrs was used to produce film thickness of about ~ 2 μm according to equation (1) [20]:

$$d = \frac{JMt}{nF\rho} \qquad (1)$$

where *d* is the film thickness, *J* is the current density (mA/cm^2), *M* is the molecular weight(g), *t* is the deposition time (sec), *n* is the number of electrons, *F* is Faraday constant (96500 C) and ρ is the CdTe density (5.85 g/cm^3). The value of *n* is taken as 2, considering the conversion of Cd^{2+} to Cd in CdTe.

The CdTe thin films were deposited at potential values of -0.6, -0.62 and -0.65 V (SCE) (Table 1).

The deposition of CdTe films on the cathode can be accomplished by the following reactions [21]:

$$HTeO_2^+ + 3H^+ + 4e^- \leftrightarrow Te + 2H_2O \qquad (2)$$

$$Cd^{2+} + Te + 2e^- \leftrightarrow CdTe \qquad (3)$$

The as-deposited CdTe film is n-type. The production of CdTe/CdS heterojunctions involved a post heat treatment step that converted n-type to p-type. Some samples that were deposited at different deposition potentials were heat treated at 400˚C in air for 15 min. Others were chemically treated using $CdCl_2$ solution and then heat treated at 400˚C in air for 15 min, followed by rinsing with distilled water and drying with nitrogen gas. CdTe films were etched using an acidic $K_2Cr_2O_7$ solution.

Table 1. CdTe samples electrodeposited at different potential values.

Deposition potential V(SCE)		Sample code
- 0.6	as-deposited	S1
	heat treatment	S2
	$CdCl_2$ + heat treatment	S3
- 0.62	as-deposited	S4
	heat treatment	S5
	$CdCl_2$ + heat treatment	S6
- 0.65	as-deposited	S7
	heat treatment	S8
	$CdCl_2$ + heat treatment	S9

The films were immersed for 2 sec in the etching solution, followed by rinsing again with distilled water and drying with nitrogen gas. For fabrication of CdTe/CdS solar cell (as shown in Figure 1), a molybdenum back electrode was deposited on the p-CdTe layer using a DC magnetron sputtering machine (Hummer 8.1, USA) with a power of 50 W for 10 min.

2.2. Characterization

The structure, composition and morphology characteristics of CdTe thin films grown on the CdS/ITO/glass substrate were investigated using XRD, Raman, EDX and SEM techniques. X-ray powder diffraction measurements were performed using Shimadzu 7000 XRD, with CuK_α radiation (λ= 1.54 Å) generated at 30 kV and 30 mA with a scanning rate of 4° min^{-1} for 2θ values between 10 and 100 degrees.

The individual crystallite size (t) was calculated using Scherrer's formula [22], as shown in equation (4)

$$t = k.\lambda /B. \cos \theta \quad (4)$$

where k is the Scherrer's constant, that is a reference value corresponding to the quality factor of the apparatus measured with a reference single crystal and dependent on the crystallite shape (0.89–0.9). λ is the X-ray wave length, B is the full width at half maximum (FWHM) or the integral width of the diffraction peak and θ is the Bragg angle [23].

Raman spectra were obtained at the excitation wavelength of 532 nm (Senterra, Germany). The surface morphology and surface homogeneity of CdTe thin films were investigated with scanning electron microscopy (JEOL, JSM-6360 LA). Composition of solid phases was estimated by energy dispersive spectrometry (EDX). The band gap energy (E_g) of CdTe films was calculated using absorbance spectra measured using a double beam UV-Vis spectrophotometer under normal incidence

in the 190 - 1100 nm wavelength range. Solar cell performance was characterized by the cell's current-voltage relationship under illumination. The current-voltage curve was determined using a solar simulator (PET Photo Emission Tech., Inc. USA) and the values of $V_{oc,}$ $J_{sc,}$ FF and η were measured.

3. RESULTS AND DISCUSSION

The properties of these films were studied as a function of the potentials, heat treatment and $CdCl_2$ treatment.

3.1. Structural analysis

3.1.1. XRD

(a)

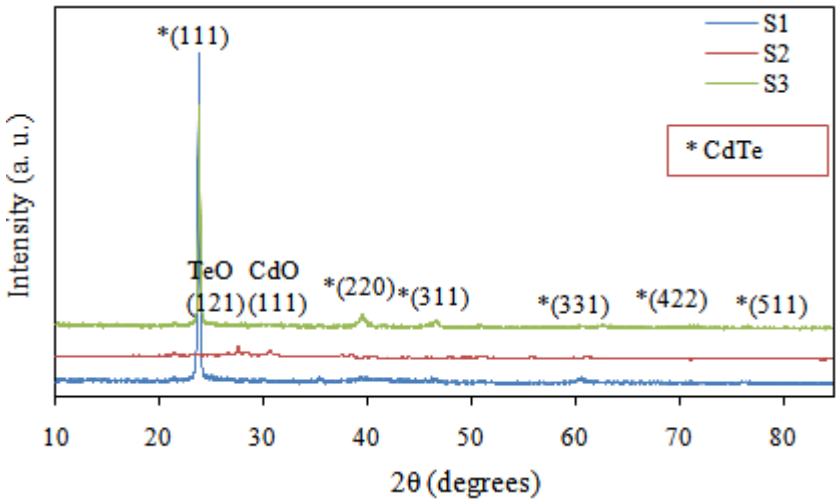

(b)

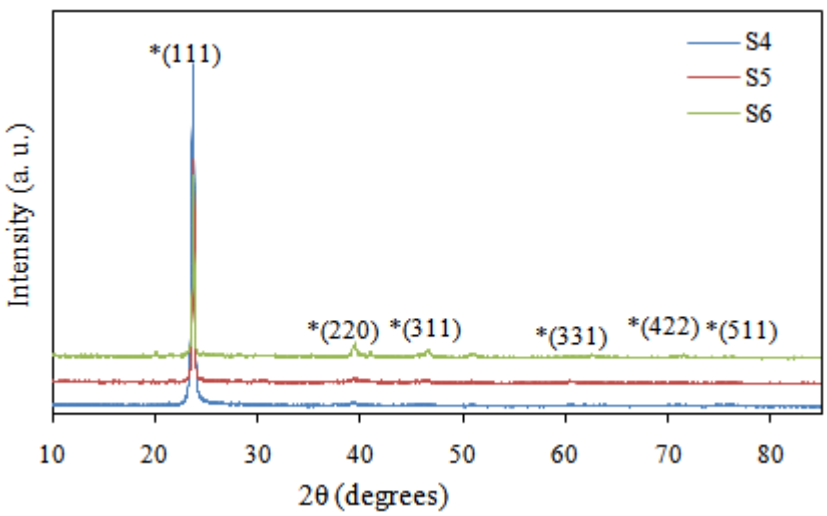

(c)

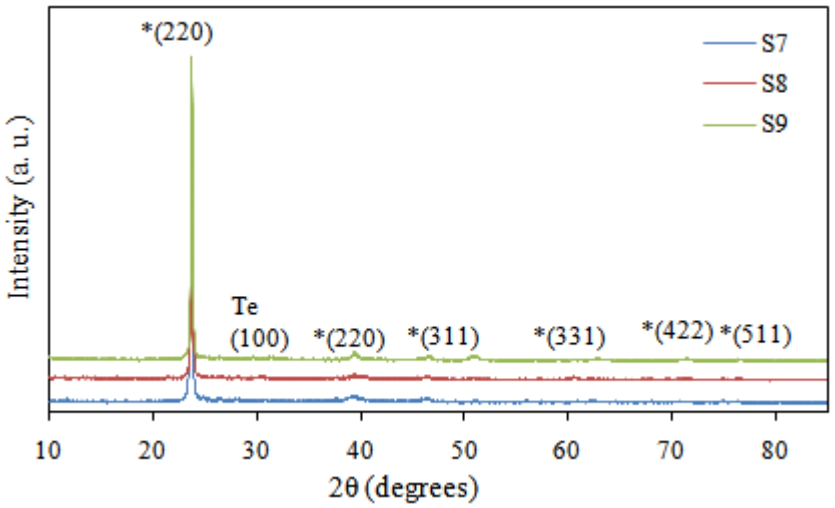

Figure 2. The X-ray diffraction patterns of as-deposited, heat and $CdCl_2$ treated CdTe thin films electrodeposited at different potential values of (a) -0.6, (b) -0.62 and (c) -0.65 V(SCE).

X-ray diffraction is used to analyze the formation of the crystalline phases. The X-ray diffraction patterns of as-deposited, heat-treated and $CdCl_2$-treated CdTe thin films on CdS/ITO/glass are shown in Fig. 2.

For samples S1, S2 and S3, CdTe films had a strong preferred orientation at 2θ of 23.7˚ corresponding to the plane parallel to the (111) direction of the cubic zinc blende structure [4]. Moreover, principal diffraction peaks at 2θ of 39.3˚, 46.4˚, 62.3˚, 71.2˚ and 76.3˚ correspond to the (220), (311), (331), (422) and (511) planes, respectively (according to JCPDS-015-0770), confirming the high crystallinity of the CdTe films electrodeposited at -0.6 V (SCE) [8]. For sample S2, the intensity of the main peak decreased and new peaks due to TeO_2 and CdO were apparent (JCPDS-42-1365 and JCPDS-65-2908) [24-25].

After $CdCl_2$ treatment (S3), the TeO_2 and CdO peaks disappeared, and the intensity of the (111) and (331) peaks decreased while the intensity of the (220) and (311) peaks increased.

Figure 2(b) showed the XRD results for the CdTe samples (S4, S5 and S6) electrodeposited on CdS/ITO/ glass substrates at the potential of -0.62 V. For the S4 sample, all peaks of the CdTe cubic zinc blend structure were obtained. After heat treatment (S5), no TeO_2 or CdO peaks were observed. The same spectrum was produced for sample S6, but the (111) peak intensity decreased, the (511) peak disappeared, and intensities of all other peaks increased.

The effect of changing the deposition potential from -0.62 to -0.65 V(SCE) is shown in Figure 2(c). According to JCPDS file no 36-1452, the S7 sample structure contained both a cubic CdTe structure and a free tellurium phase [26]. The (111) plane peak intensity of S7 was lower than those of S1 and S4. The intensity of all peaks decreased after the heat treatment (S8). For sample S9, the

intensity of the (111) peak as well as of the other peaks increased and the free tellurium phase disappeared. Because of the $CdCl_2$ treatment, the XRD peaks became sharper and more identified.

The calculated crystallite size of samples S3, S6 and S9 using Scherrer's formula for (111) plane according to equation (4) is shown in Figure 3. The crystallite size of the $CdCl_2$ treated CdTe films increased as the deposition potential increased from -0.6 V(SCE) to -0.62 V(SCE) and then decreased at the deposition potential of -0.65 V (SCE).

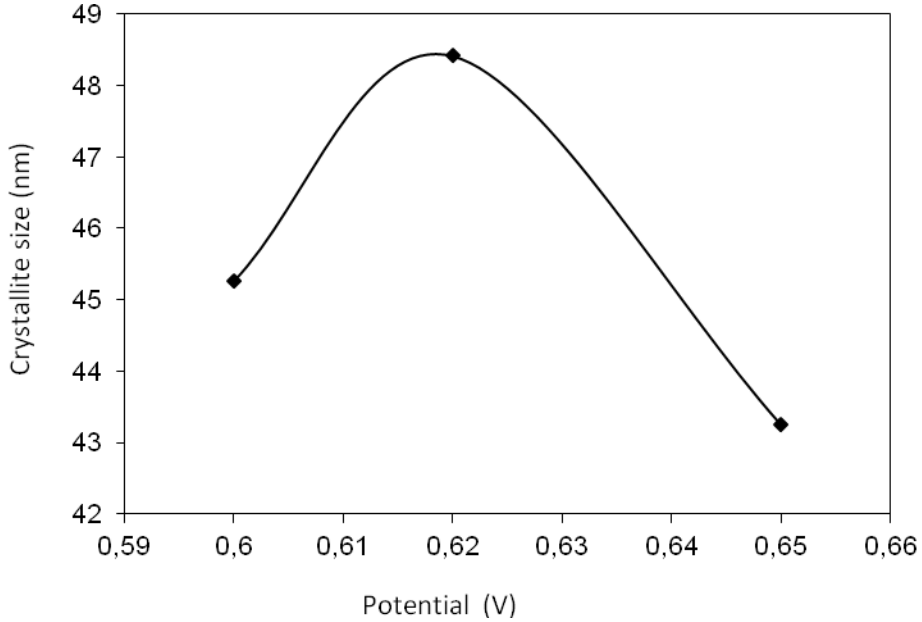

Figure 3. Dependence of crystallite size on the deposition potential.

3.1.2. Raman analysis

The molecular structure and identification of phases in CdTe films were explored using Raman spectra. The Raman spectra of different samples (Table 1) are shown in Figure 4. For all samples, five energy peaks were observed at 120, 130, 140, 151 and 170 cm^{-1}. The positions of all of the peaks are very close to those reported by other researchers in the field [27-29].

Peaks at 170, 151 and 140 cm^{-1} were observed for all CdTe bulk crystals, . The peaks at 170 and 140 cm^{-1} correspond to the longitudinal (LO) and the transverse (TO) modes, whereas the peak at 151 cm^{-1} lies between the two modes [30]. The peak at 120 cm^{-1} is related to the TeO_2 Raman vibrational mode. The entire film area was tested point by point and showed no significant changes among the different spectra, indicating a good homogeneity of the deposited film. For all samples, the Raman spectra intensities were enhanced after the heat and $CdCl_2$ treatments [31-32].

For samples electrodeposited at -0.6 V(SCE) (S1, S2 and S3), the appearance of the peak at 130 cm^{-1} for sample S3 is due to the vibrations in the tellurium inclusions [30].

For samples electrodeposited at -0.62 V(SCE) (S4, S5 and S6), the 130 cm^{-1} peak was reduced gradually. This indicates that S6 contains a lower amount of free Te than S4 and S5, whereas by increasing the electrodeposition potential to -0.65 V(SCE), the energy peak at 130 cm^{-1} once again

became obvious and more intense after the heat and $CdCl_2$ treatments. This result was in agreement with the data previously obtained from XRD measurements.

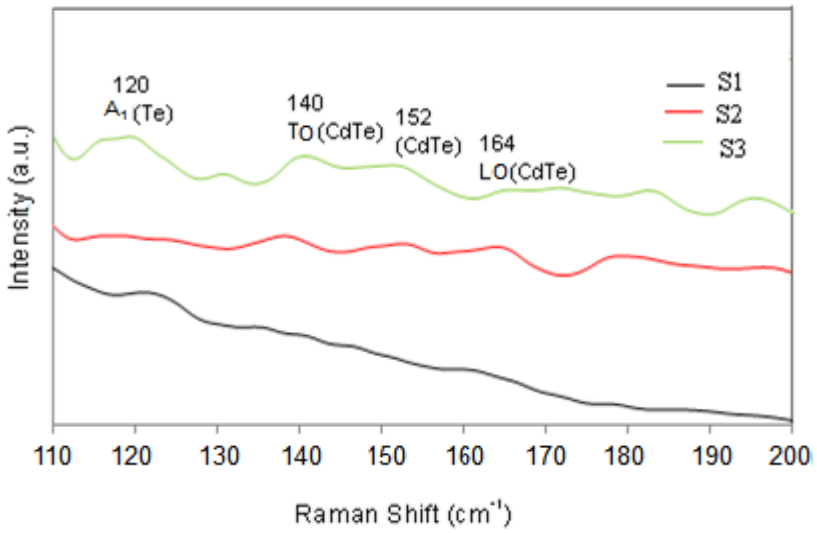

(a)

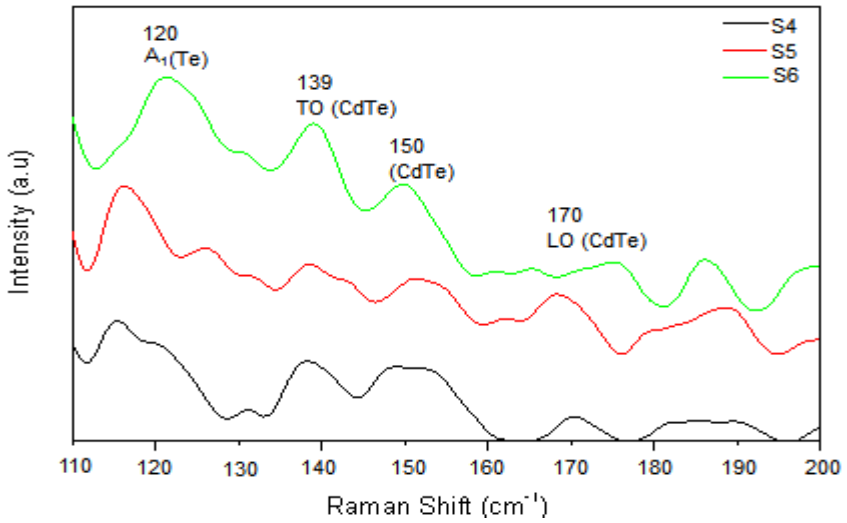

(b)

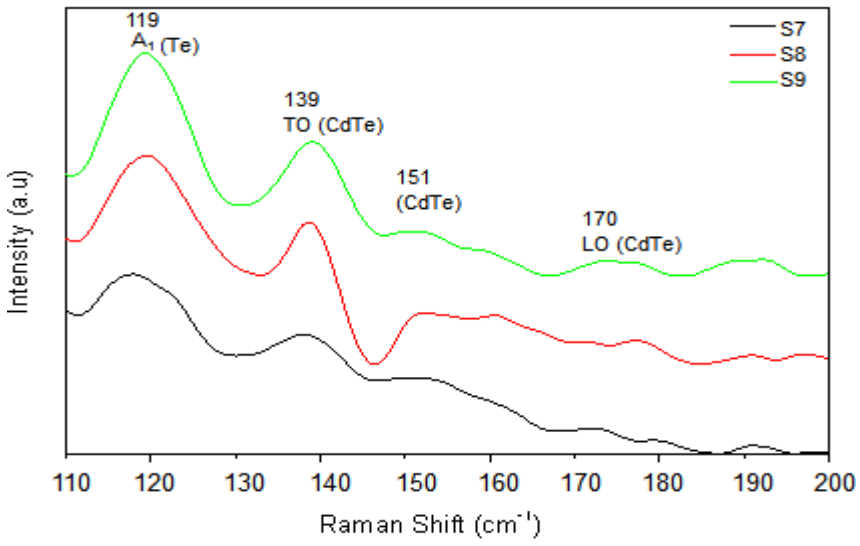

(c)

Figure 4. Raman spectra of the as-deposited, heat and $CdCl_2$ treated CdTe thin films electrodeposited at different potential values: (a) -0.6, (b) -0.62 and (c) -0.65 V(SEC).

3.2. Morphological analysis

Figure 5 shows the SEM images of all CdTe samples listed in Table 1. For as-deposited CdTe samples at different potentials (S1, S4 and S7), small particles were aggregated and form well connected grains [33] with the grain size decreasing with increased electrodeposition potential magnitude. The SEM images also indicated that the growth process occurred predominantly by grain growth and not through the layer by layer mode [21]. The heat treatment process reduced particle aggregation in samples S2 and S8, but S5 still exhibited a granular structure closely grown on the surface [34]. After $CdCl_2$ treatment (S3, S6 and S9), the particle size was increased for samples S3 and S9 and the grain size increased for sample S6. In general, the $CdCl_2$ treatment increased the surface roughness and improved the shapes of the grains and the particles, making them more defined.

The compositions of CdTe thin films were studied by EDX with the results presented in Table 2. It was observed that the as-deposited samples (S1, S4 and S7) became slightly richer in Te as was previously reported in [34]. After the heat and $CdCl_2$ treatment, the Te ratio in the samples decreased. Additionally, composition analysis showed that compared to the other samples, sample S6 was nearly stoichiometric. This suggests that the deposition potential plays a crucial role for the control of the film deposition properties [35].

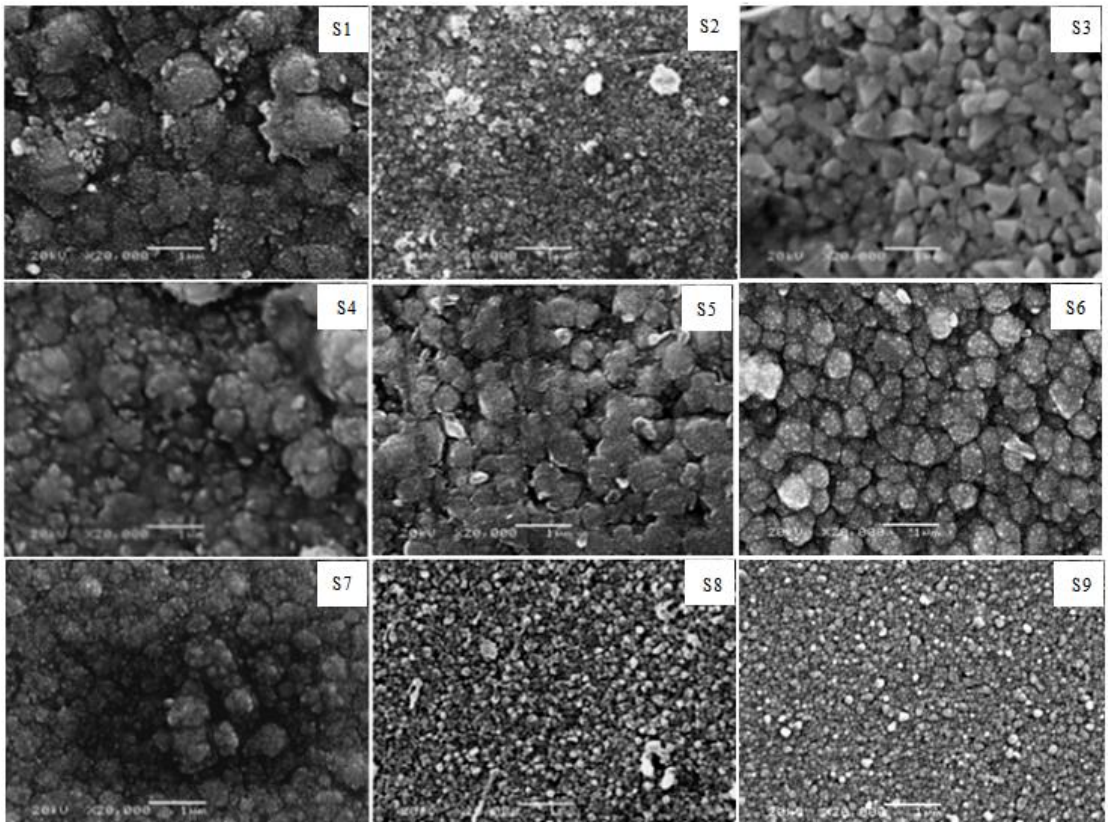

Figure 5. SEM images of the as-deposited, heat and $CdCl_2$ treated CdTe thin film surfaces electrodeposited at different potential values.

Table 2. The composition analysis (Atomic %) and the band gap energy of CdTe samples

Deposition potential V(SCE)	Sample	Cd %	Te %	E_g (eV)
- 0.6	S1	40.1	59.9	1.46
	S2	61	39	1.24
	S3	46.9	53.1	1.4
- 0.62	S4	42	58	1.42
	S5	51.33	48.67	1.45
	S6	**50.38**	**49.62**	**1.44**
- 0.65	S7	44.5	55.5	1.4
	S8	49.1	50.9	1.41
	S9	44.5	55.5	1.43

3.3. Optical analysis

The absorption spectra of the CdTe samples were obtained in the 190-1100 nm wavelength range, and the absorption coefficients for each wavelength were calculated from the absorption spectroscopic data.

CdTe is a direct band gap material [36, 37] and the relation between the optical absorption coefficient (α) and the incident photon energy is:

$$(\alpha h\nu)^2 \alpha (h\nu - E_g) \quad (5)$$

where ν is the frequency of the incident photons, hν is the photon energy and E_g is the band gap energy.

Based on this equation, the band gap energy can be obtained from the intercept of the plot on the X-axis; the E_g values obtained this way for all CdTe films are presented in Table 2.

We observed that the band gap energies for all samples are approximately 1.4 eV and in particular the E_g for sample S6 was 1.44 eV; the excellent agreement with the reported bulk CdTe band gap value [13, 38] supports the stoichiometry of Cd:Te deposition for sample S6.

3.4. J-V curve

Based on the results discussed above, we concluded that sample S_6 has a high crystallinity, does not include any free Te, exhibits the most defined grains and is nearly stoichiometric with a band gap of 1.44 eV. The fabricated CdTe/CdS solar cell was therefore based on the S6 sample. The cell exhibits the following photovoltaic properties for cell area of 0.08 mm^2 illumination intensity of 100 mW/cm^2: an efficiency (η) of 9%, open circuit voltage (V_{oc}) of 0.73 V, short circuit current density (J_{sc}) of 20 mA/cm^2, and fill factor (FF) of 50%.

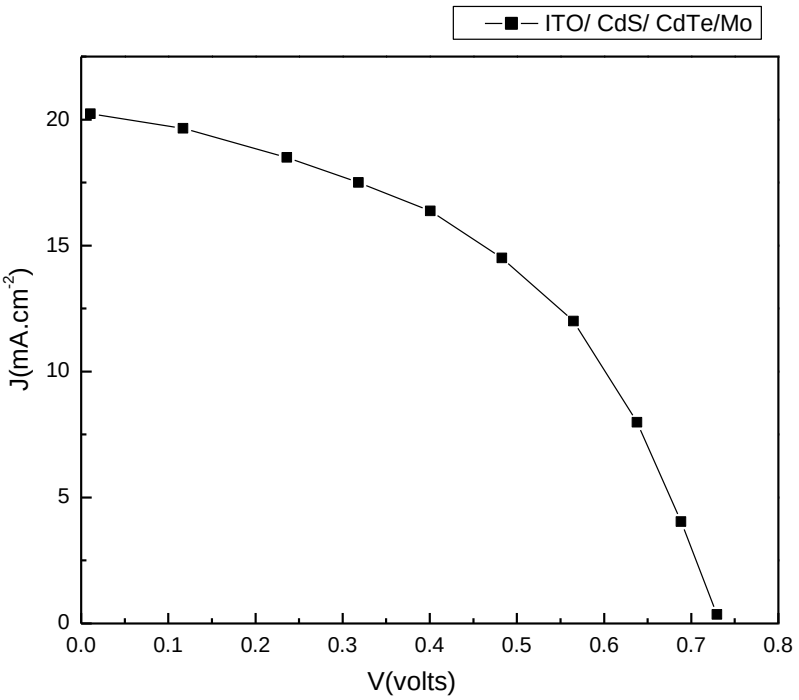

Figure 6. The J - V curve of CdTe/CdS solar cell.

4. CONCLUSIONS

The individual effects of electrodeposition potential variation, heat treatment, and $CdCl_2$ treatment on the properties of CdTe films deposited on CdS/ITO substrates have been investigated. Nanocrystalline CdTe films with cubic zinc blende structure were produced using -0.6, -0.62, and -0.65 V (SCE) potentials. A decrease in the grain sizes and Te-rich samples were obtained as the magnitude of the potential increased. However, no grain growth and no free Te were observed after heat treatment and $CdCl_2$ treatment, especially for the film deposited at -0.62 V(SCE). Thus, the heat and CdTe treatment was found to be necessary to improve the film stoichiometry and quality that affect the efficiency of CdTe/CdS solar cells.

CdTe thin films have been successfully deposited on CdS/ITO substrates from an aqueous solution by using the electrodeposition technique. To simplify the processing and eliminate a potential source of impurities, the electrodeposition was performed using the 3-electrode system. Structural analysis showed that the heat and $CdCl_2$ treated CdTe film had a high crystal quality and high preferential orientation along the (111) plane. SEM characterization indicated that the growth process occurs predominantly by cluster growth and not through layer by layer mode. Composition analysis of the films showed that the heat and $CdCl_2$ treated CdTe thin film was nearly stoichiometric. Using optical analysis, it was found that the CdTe thin films had a direct band gap of approximately 1.44 eV. After the fabrication of a solar cell, photovoltaic energy conversion characteristics were investigated under illumination of 100 mW/cm^2 and an efficiency of 9% was observed.

ACKNOWLEDGEMENT
A part of this work has been supported by the Ministry of Scientific Research, Egypt, under the Science and Technology Development Fund Program (STDF), project ID: 1396 with the title "Synthesis of thin films to produce photovoltaic solar cells".

References

1. S. Chun, S. Lee, Y. Jung, J. S. Bae, J. Kim, D. Kim, *Current Applied Physics* 13 (2013) 211.
2. D.H. Rose, F.S. Hasoon, R.G. Dhere, D.S. Albin, R.M. Ribelin, X.S. Li,Y. Mahathongdy, T.A. Gessert, P. Sheldon, *Progress in Photovoltaics: Research and Applications* 7 (1999) 331.
3. X. Wu, R.G. Dhere, D.S. Albin, T.A. Gessert, C. Dehart, J.C. Keane, T.J. Coutts,S. Asher, D.H. Levi, H.R. Moutinho, Y. Yan, T. Moriaty, S. Johnston, K. Emery,P. Sheldon, *National Renewable Energy Laboratory* (NREL) 250 (2001) 31025.
4. V. Barrioz, G. Kartopu, S.J.C. Irvine, S. Monir, X. Yang, *Crystal Growth* 354 (2012) 81.
5. S. Chun, K.-S. Han, J.-H. Shin, H. Lee, D. Kim, *Crystal Growth* 87 (2010) 2097.
6. B.E. McCandless, R.W. Birkmire, *Solar Cells* 31 (1991) 527.
7. B. M. Basol, *J Appl. Phys*. 58 (1985) 3809.
8. M. Soliman, A.B. Kashyout, M. Shabana M. Elgamal, *Renewable Energy*, 23 (2001) 471.
9. T.L. Chu, S.S. Chu, C. Ferekids, C.Q. Wu, J. Britt, C. Wang, 22nd IEEE Photovoltaic Specialists Conference, Las Vegas, Nevada, October 7–11, (1991) 952.

10. S.P. Albright, B. Ackerman, R.R. Chamberlin, J.F. Jordan, National Renewable Energy Laboratory (NREL) (1991) Subcontract ZN-9-19019.
11. T. Arita, A. Hanafusa, S. Kitamura, H. Takakura, M. Murazono, Large area CdS/CdTe solar cells.Conference record of the 22nd IEEE Photovoltaic Specialists Conference, Las Vegas, Nevada, October 7–11, (1991) 946.
12. J. Skarp, Y. Koskinen, S. Lindfors, A. Routiainen, T. Sountola. In: Proc. 10th European Photovoltaic Solar Energy Conference, Lisbon, Porugal, April 8–12. Dordrecht: Kluwer, (1991) 567.
13. F. Abou-Elfotouh, M. Soliman, AE. Riad, M. Al-Jassim, Coutts, 22nd IEEE Photovoltaic Specialists Conference, Las Vegas, Nevada, October 7–11(1991) 1109.
14. H. Bayhan, C. Ercelebi, *TUBITAK*, 22 (1998) 441.
15. J. Saraie, M. Kitagawa, M. Ishida, T. Tanaka, *Crystal Growth* 43 (1978) 13.
16. D.W. Niles, D. Waters, D. Rose, *Applied Surface Science* 136 (1998) 221.
17. S. Vatavu, H. Zhao, V. Padma, R. Rudaraju, D.L. Morel, P. Gasin, Iu. Caraman, C.S. Ferekides, *Thin Solid Film* 515 (2007) 6107.
18. A.B. Kashyout, M. Fathy, M. B. Soliman, *International J. Photoenergy*, Article ID 139374 (2011) 1.
19. M.Fathy, A.B. Kashyout, Sh. Elyamny, G. D. Roston, A. A. Bishara, *Int. J. Electrochem. Sci*. 9 (2014) 6155.
20. K.R. Chauhan, Ian J. Burgess, Gap Soo chang, I. Mukhopadhyay, *J. Electroanalytical Chemistry* 11(2013) 32.
21. B.M. Basol, Solar Cells 23 (1988) 69.
22. B. D. Cullity, Elements of X-Ray Diffraction, 2nd ed. Addison Wesley, U.S.A. (1978) Chap. 3, 102.
23. S. Chun, Y. Jung, J. Kim, D. Kim, *Crystal Growth*, 326 (2011) 152.
24. G. Subodh and M. T. Sebastian, *Japanese Journal of Applied Physics* 47 (2008) 7943.
25. V. Veeraputhiran, V. Gomathinayagam, A. Udhaya, K. Francy, B. Kathrunnisa, *Advanced Chemical Sciences* 1 (2015) 17.
26. P. Mohanty, J. Park, and B. Kim, *Nanoscience and Nanotechnology* 6 (2006)1.
27. Y. Jung, S. Chun, D. Kim and J. Kim, *J. Crystal Growth* 326 (2011) 69.
28. J. Rouusset, E. Rzepka, D. Lincot, *J. Phys. Chem*. B 113 (2009) 4333.
29. R. Ochoa-Landin, O. Vigil-Galan, Y. V. Vorobiev and R. Ramirez-Bon, *Sol. Energy Mat. Sol. Cells* 83 (2009) 134.
30. V. S. Vinogradov, G. Karczewski, I. V. Kucherenko, N. N. Mel'nik, P. Fernandez, *Physics of the Solid State*, 50 (2008) 164.
31. P. Nozar, G. Mittica, S. Milita, C. Albonetti, F. Corticelli, A. Brillante, I. Bilotti, G. Tedeschi, C. Taliani, *MRS Proceedings*, 1447 (2012).
32. J. Huerta-Ruelas, M. Lopez-Lopez, O. Zelaya-Angel, *Jpn. J. Appl. Phys*. 39 (2000) 1701.
33. M. Miyake, K. Murase, T. Hirato, Y. Awakura, *Surface and Coatings Technology*, 169 –170 (2003) 108.
34. M. Miyake, K. Murase, T. Hirato, Y. Awakura, *J. Electroanalytical Chemistry* 562 (2004) 247.
35. K. Zanio, Semiconductors and Semimetals, Academic press 13 (1978).
36. S. Lalitha, R. Sathyamoorthy, S. Senthilarasu, A. Subbarayan , and K. Natarajan, *Sol. Energy Mater. Sol. Cells* 82 (2004)187.
37. R. Sathyamoorthy, S. K. Narayandass, and D. Mangalaraj ,*Sol. Energy Mater. Sol. Cells* 76 (2003) 339.
38. E. Fatus, P. Herrasti, T. Garcia, F. Arjona and E.G. Camarero, *Muter.Chem. Phys*., 13 (1985) 497.